A Planar Variable Reluctance Magnetic Micromotor with Fully Integrated Stator and Coils

Chong H. Ahn, Yong J. Kim, and Mark G. Allen, *Member, IEEE*

Abstract—**A fully functional electrically excited planar variable reluctance magnetic micromotor has been demonstrated on a silicon wafer. The motor uses a micromachined nickel-iron rotor and a fully integrated stator, in which a toroidal-meander type integrated inductive component is used for flux generations. To reduce the magnetic reluctance in the stator, a modified stator geometry was adopted which removes the yoke used in a conventional magnetic variable reluctance motor. Using polyimide as both an integral structural material as well as an electroplating mold, a 40-μm-thick nickel-iron rotor 500 μm in diameter was microassembled onto a fully integrated nickel-iron stator 120 μm in thickness. When 500 mA of current was applied to each stator, 12° of rotation (1 stroke in this motor) was observed. By applying three phase 200-mA current pulses to the stators, rotation of the rotor was observed. The speed and direction of the rotation could be adjusted by changing the frequency and phase firing order of the power supply, respectively. Continuous rotor rotation was observed at speeds up to 500 rpm; this speed limitation was solely due to the limitation of the maximum frequency of the controller used. The micromotor could be reproducibly started, stopped, reversed, and continuously rotated. The predicted torque for the fabricated micromotor at 500-mA driving current was calculated to be 3.3 nN-m.**

I. Introduction

RECENTLY there has been much work towards realizing practical micromotors using different operating principles for a variety of applications. These efforts have focused mainly on electrostatic drive [1], [2], but ultrasonic [3], dielectric induction [4], and magnetic drives [5], [6] have also been investigated. Among these proposed operating principles, magnetic drive is attractive in applications such as conductive fluids for some biomedical applications, or operation in environments where high driving voltages are unacceptable or unattainable.

In previous work towards realizing a magnetic-based micromotor, hybrid techniques have been used to either place permanent magnetic components onto integrated planar coils [5] to introduce external magnetic fields onto integrated high-permeability moving parts [6], or to use hybrid wire-bonding techniques to create coils [7]. One reason these approaches have been taken is the difficulty in fabricating three-dimensional "wrapped" coils using an integrated, planar fabrication process. However, recently, a new planar integrated meander-type inductive component was proposed and demonstrated [8]–[11], in which multilevel magnetic cores were "wrapped" around planar meander conductors. This configuration can be thought of as the result of interchanging the roles of the conductor wire and magnetic core in a conventional inductor. A schematic drawing of a section of the integrated toroidal-meander type inductor is shown in Fig. 1. With this integrated inductive component, it is possible to guide magnetic flux confined in an integrated magnetic core to the locations where magnetic actuation or sensing take place. This integrated inductive component makes it possible to fabricate a magnetic microactuator in a fully integrated fashion; such a device using a movable cantilever beam has recently been demonstrated [9].

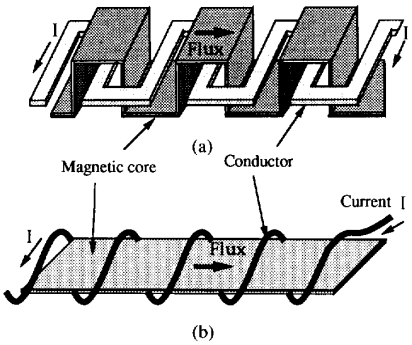

Fig. 1. Schematic diagrams of the integrated meander-type inductor and the conventional toroidal-type inductor. The structure of the two inductor schemes is analogous: (a) meander-type inductor; (b) conventional toroidal-type inductor.

In particular, using this component as the basis for a micromotor stator to generate magnetic flux, a fully functional, electrically excited planar variable reluctance magnetic micromotor has been demonstrated on a silicon wafer [10]. This motor has a similar operating principle to the conventional magnetic variable reluctance motor. For a preliminary demonstration, stators (with fully integrated coils) and rotors are fabricated separately, and then assembled together using microassembling techniques, although the process used for fabrication is completely compatible with fully integrated devices.

Manuscript received July 14, 1993; revised December 15, 1993. Subject Editor, R. O. Warrington. This work was supported by the National Science Foundation under Grant ECS-9117074.

The authors are with the School of Electrical and Computer Engineering, Microelectronics Research Center, Georgia Institute of Technology, Atlanta, GA 30332-0269.

IEEE Log Number 9215841.

II. Magnetic Material and *In Situ* Measurement of Magnetic Properties

In designing a planar magnetic microactuator, magnetic material properties measured from bulk-type samples may not be useful since these properties may depend on film geometry, thickness, and size. In particular, the magnetic core structure to be used in this research is a multileveled meander-type core [8], [9] which has a different geometry and size from a bulk-type or a simple film-type magnetic core. Thus, before designing a magnetic micromotor, the magnetic properties of the multilevel meander core should be understood. In measuring the magnetic properties of the film core used for a microstructure, it is important to remember that the properties of interest must be measured *in situ*; that is, on as-deposited films.

Although there are several different types of soft magnetic materials, those which are available in thin film form are of interest in this research. Among the available soft magnetic materials, nickel-iron (Ni/Fe) permalloy has been used as a promising material in a variety of magnetic film applications, since it has favorable magnetic [8], [11] as well as mechanical [13] properties for magnetic actuator applications [9]–[11].

It was reported that both the mechanical [13] and the magnetic properties [12], [14] of the applied permalloy are affected greatly by the material compositions used. In particular, the composition of Ni(81%)/Fe(19%) film can meet the requirements as an appropriate material for microactuator applications because this composition can simultaneously achieve maximum permeability, minimum coercive force, minimum anisotropy field, and maximum mechanical hardness. Thus, this composition was chosen in this research. This permalloy can be deposited by using either evaporation or electroplating, but in this research the electroplating technique is adopted due to the cost advantage in making a film of several tens of micrometers. For the electroplating, a plating bath was built using the compositions shown in Table I [12], [14].

Permeability test samples were then prepared using surface micromachining techniques. Thus, an *in situ* measurement was performed in the sense that the test samples have the same geometry and dimension as the film deposited in the actual inductor, without inducing any distortions in mechanical and electrical properties in preparing the samples. To prepare test samples, the fabrication sequence, which is similar to the fabrication steps described later in this paper, is shown in Fig. 2. This fabrication was performed using the same fabrication mask sets which are to be used in the fabrication of magnetic components. Thus, the prepared test samples have exactly the same sizes and the same geometries as the magnetic films used in the actual components. The geometry of test samples which were prepared for *in situ* measurement in this research was a multilevel meander-type film.

The magnetic property of greatest interest in this research is the relative magnetic permeability and the saturation flux density in the easy axis [12], [14]. If the easy axis of a magnetic film is not induced in a specific direction (e.g., by applied magnetic field during deposition), it is usually produced in parallel to the surface of the substrate on which the film is formed. However, the permeability of a magnetic material has nonlinear characteristics with respect to the applied magnetic flux density which must also be assessed. These can be described through the B-H relationship for the magnetic material.

TABLE I
Composition of the Nickel-Iron and Copper Electroplating Solutions

Nickel-Iron Permalloy		Copper	
Component	Quantity (g/l)	Component	Quantity
$NiSO_4 \cdot 6H_2O$	200	$CuSO_4 \cdot 5H_2O$	1200 (g/l)
$FeSO_4 \cdot 7H_2O$	8	H_2SO_4	100 (ml/l)
$NiCl_2 \cdot 6H_2O$	5		
H_3BO_3	25		
Saccharin	3		

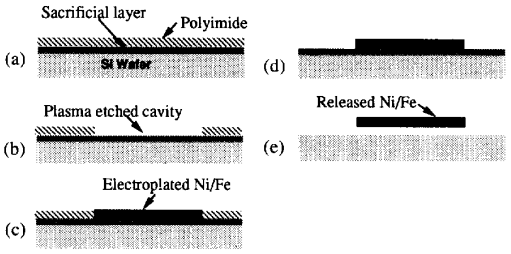

Fig. 2. Fabrication sequence of the test samples for the *in situ* measurement of magnetic properties: (a) sacrificial layer and polyimide deposition; (b) cavity etching; (c) nickel/iron plating; (d) polyimide etching; (e) nickel/iron release.

The B-H curves were obtained from magnetization (or moment) versus applied field curves which are measured by using a vibrating sample magnetometer (Model 4500, Lake Shore Cryotronics, Inc.). Fig. 3 illustrates the magnetization of the multilevel meander-type film as a function of applied DC field for low field measurements. As shown in Fig. 3, the easy axis is generated in the direction parallel to the surface of the core, whereas the hard axis is built in the normal direction to the surface. The slope of the easy axis in the linear regime is steeper than that of the hard axis, indicating that the easy axis achieves higher effective permeability. These magnetization data are used to calculate the relative permeability of the film samples:

$$\mu_r = \frac{\mu}{\mu_0} = 1 + \frac{M_v}{H_{\text{int}}} \tag{1}$$

where M_v is the volume magnetization and $H_{\text{int}} = H_{\text{app}} - DM_v$ is the internal field, in which H_{app} is the externally applied field and D is the sample demagnetization factor.

To find the relative permeability of the meander-type magnetic core, computations were performed for the easy axis at the "linear" portion (i.e., the ascending and descending branches near ± 0.2 emu) of the low field magnetization data shown in Fig. 3. The weight of the test

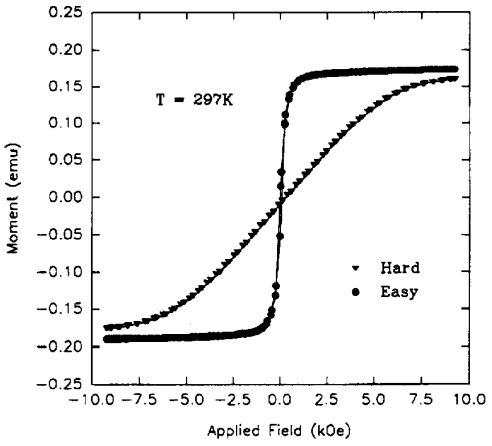

Fig. 3. Magnetization (emu) as a function of applied dc field using the low field measurements for the multilevel meander-type core.

sample is 0.6 mg and the density of Ni(81%)/Fe(19%) is assumed as 8.9 g/cm^3. If these calculation steps are repeated in a piecewise linear fashion on the magnetization (or moment) versus applied field curves, the permeability of a test material as a function of the applied field can be found. Using the obtained permeability as a function of the applied magnetic field, the entire B-H curve of the test sample can be drawn. From the B-H values evaluated from the results shown in Fig. 3, the meander-type magnetic core is saturated at approximately 0.5 T and the evaluated relative permeability μ_r shows 500 at the linear region. It should be emphasized that the above calculation assumes zero demagnetization effect. Note that the relative permeability and flux saturation at high frequencies (approximately 1 MHz) may have different values from those which are obtained at low frequencies (from DC to 10 kHz) in this section.

III. Micromotor Design

A variable reluctance magnetic motor has two sets of salient poles, one set in the stator (which usually has excitation coils wrapped around the magnetic poles) and another set on the rotor. This motor requires no permanent magnets to produce a torque moment. The stator coils arranged in one or more sets and phases should be excited individually or in pairs to produce torque for rotor rotation. When a phase coil is excited, the nearest rotor poles located to the excited stator poles are attracted to the stator poles. Due to the rotation of the rotor, when the rotor poles are aligned with the excited stator poles, the excited phase should be switched off and the next phase is then excited to maintain continuous rotor rotation.

A conventional variable reluctance magnetic motor as shown in Fig. 4(a) consists of the rotor and the stator, where the stator contains a magnetic yoke to form a magnetic path from one stator pole through the rotor and the stator pole directly across from the first pole, and back around the yoke to the first pole. This works well in conventional motors since the reluctance of the yoke can usually be neglected. However, in contrast to conventional magnetic circuits, a micromachined magnetic circuit usually has a high magnetic reluctance due to processing limitations on the achievable permeability and/or thickness of the magnetic core. In fact, in many micromagnetic actuators, the reluctances of the core and air gap can be comparable [11], [15]. Thus, reduction of the core reluctance is a major concern in realizing a micromachined magnetic circuit. If the permeability cannot be increased, the geometry must be modified. The major geometric factors which affect the reluctance in a magnetic core are the core cross-sectional area and length. Since the core cross-sectional area is usually limited by planar geometric constraints, one of the best design strategies to reduce the reluctance is to shorten the length of the core.

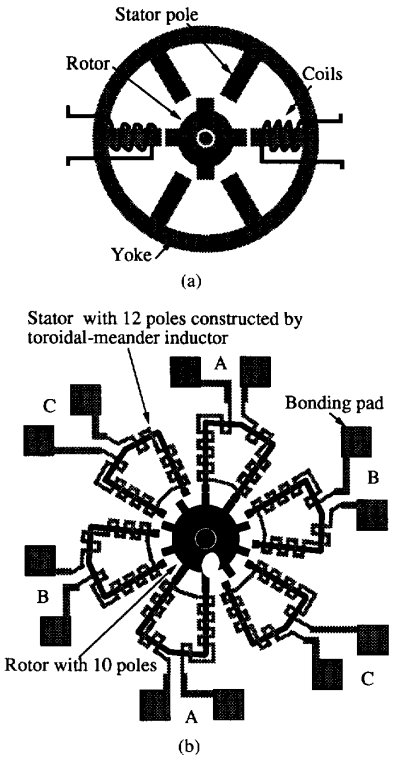

Fig. 4. Structure of conventional and modified variable reluctance motors. (a) Schematic diagram of the magnetic core of a conventional magnetic variable reluctance motor showing the yoke frame; (b) schematic diagram of modified planar variable reluctance magnetic motor fabricated in this research. The structure consists of 12 stator poles and 10 rotor poles in three phases. Each magnetic core is separated from the others.

This motivation to minimize core reluctance makes it desirable to modify the standard variable reluctance motor design [16], since the long magnetic path through the yoke adds significantly to the core reluctance. A schematic diagram of the modified design is shown in Fig. 4(b). The wound poles of all phases are arranged in pairs of opposite polarity to achieve adjacent pole paths of short lengths. The stator poles are positioned so as to greatly shorten the magnetic flux paths and to provide an isolated magnetic core for the flux path of each phase. This isolated mag-

netic circuit reduces the core reluctance by 50% [11]. In addition, it is possible to wind coils on the outside of the core, which increases both the number of turns which can be achieved as well as allowing the bonding pads to be on the periphery of the motor.

The poles are wound oppositely in pairs to form the phases. Each phase then produces a pulse of torque on each passing rotor pole. The fundamental switching frequency f to rotate a rotor with a speed n (rev/s) is

$$f = nN_r \tag{2}$$

where N_r is the number of rotor poles.

If a motor has q phases, qN_r steps are required per revolution, where the "stroke" (or "step angle") is

$$S = \frac{2\pi}{qN_r} \quad \text{(rad)}. \tag{3}$$

One feasible design for a magnetic micromotor with no external yoke (which will be fabricated below) has 12 stator poles and 10 rotor poles (12/10) in 3 phases (as opposed to a conventional 12 stator pole/8 rotor pole design), and has 12° of rotation per stroke. As shown in Fig. 4(b), two stator pole pairs in the same phase are placed in the opposite locations across the rotor, where each stator pole pair contains 7 turns of toroidal-meander coil. The angle between rotor poles is 36°, the angles between stator poles are 36° for those located in the same phase and 24° for those located in the nearby different phase, respectively (i.e., stator angles of 36°/24°), and the required strokes per revolution is 30. Table II shows a list of other feasible pole arrangements for this type of motor design.

TABLE II
SOME POSSIBLE ROTOR/STATOR POLE COMBINATIONS FOR THE MOTOR SHOWN IN FIG. 4(b)

Number of Phases	Stator/ Rotor Poles	Strokes per Rotation	Rotor Angle (degree)	Stator Angles (degree)
2	4/3	6	120	120/60
3	6/5	15	72	72/48
3	12/10	30	36	36/24
4	16/14	48	25.7	25.7/38.6
5	10/9	45	40	40/32

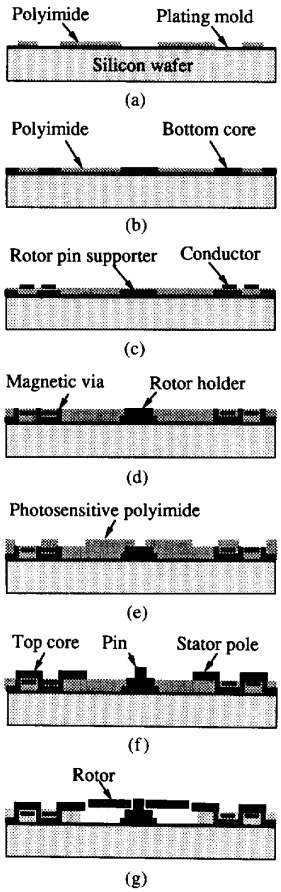

Fig. 5. Fabrication sequence for the magnetic micromotor: (a) polyimide deposition, dry etching; (b) bottom core electroplating; (c) patterning of conductor; (d) magnetic via and rotor pin electroplating; (e) photosensitive polyimide deposition and developing; (f) top core and stator pole electroplating; (g) rotor and stator microassembly.

IV. FABRICATION

The stator and pin were fabricated using a polyimide multilevel metal interconnection technique, in which an electroplated high permeability nickel(81%)-iron(19%) permalloy was used as the magnetic material.

The fabrication process of this micromotor is shown in Fig. 5. The process started with 3-in ⟨100⟩ silicon wafers as a substrate, onto which 0.6 μm of PECVD silicon nitride was deposited. Onto this substrate, chromium (500 Å)/copper (2000 Å)/chromium (700 Å) layers were deposited using electron-beam evaporation to form an electroplating seed layer.

Polyimide (Dupont PI-2611) was then spun on the wafer in multiple coats to build electroplating molds for the bottom magnetic core. Four coats were used to obtain a 40-μm-thick polyimide film. Each coat was cast by continuous two-step spin speeds: 700 rpm for 10 s and then 3000 rpm for 4 s. The wafer was then soft baked for 10 min at 120°C prior to the application of the next coat. After the deposition of all coats, the polyimide was cured at 350°C for 1 h in nitrogen, yielding an after-cure thickness of 40 μm. Holes which contained bottom magnetic cores were etched in this polyimide using a 5% CF_4/O_2 plasma etch and an aluminum hard mask until the chrome/copper/chrome seed layer was exposed.

The electroplating forms were then filled with nickel(81%)-iron(19%) permalloy using standard electroplating techniques [12], [14] and the nickel-iron electroplating bath described in Table I. To electroplate the bottom magnetic cores, electrical contact was made to the seed layer, and the wafers were immersed in the plating solution. During the electroplating, the solution was maintained at room temperature and a pH of approxi-

mately 2.7, and was stirred very slowly with a Teflon propeller blade. An applied current density of 2 mA/cm^2 resulted in an electroplating rate of 0.1–0.15 μm/min. In order to insulate the bottom magnetic core from the conductor coil, polyimide was spin coated (as above) with two step speeds and hard cured at 350°C for 1 h.

To construct a thick planar meander conductor coil, copper was plated through a thick photoresist mold. A chromium (500 Å)/copper (2000 Å)/chromium (700 Å) seed layer was deposited, and a 60-μm-wide copper plating mold was formed in 8-μm-thick positive photoresist. The copper conductors were plated through the defined molds using standard electroplating techniques and the copper plating solution described in Table I.

To facilitate gold wire bonding for the final test, a 0.5-μm-thick layer of gold was plated on the top of the plated copper conductor coils and bonding pads using a commercial cyanide-based gold plating bath. The measured resistance of the conductor coil per stator was approximately 1.5 Ω. Note that the bottom magnetic core is electrically isolated from the plating solution during this step. Upon completion of the electroplating, the photoresist was removed with acetone, and the copper seed layer was etched in a sulfuric-acid-based copper etching solution.

In order to insulate the conductor line and replanarize the surface, one coat of polyimide, approximately 10 μm in thickness, was deposited and cured as described above. Via holes were then dry etched through the polyimide layer between the meander conductors using 100% oxygen plasma and an aluminum hard mask. Upon completion of the via etch, the aluminum hard mask was removed. Because the bottom magnetic core was exposed to the oxygen plasma during dry etching, the surface of the magnetic core was oxidized. To remove the oxide film, the exposed areas of the bottom magnetic cores were etched in a 2% hydrofluoric acid solution for 30 s. Contact was then made to the bottom magnetic core, and the vias were filled with nickel–iron using the electroplating bath and conditions described previously.

Upon completion of the via electroplating, an evaporated nickel seed layer was defined between the magnetic vias using a lift-off technique for the electroplated top cores. A 1000-Å chromium layer was then deposited as a dummy seed layer to provide a uniform magnetic top core plating and to protect the defined nickel seed layer. Stator poles, rotor pins, and top magnetic cores were processed on the same level, which required high aspect ratio structures.

In order to obtain high aspect ratio patterns, photosensitive polyimide 40 μm in thickness was used as a plating mold for the top patterns of both stators and rotors. Photosensitive polyimide processing [17] has already been demonstrated to construct a 100-μm-thick structure with a high aspect ratio of 8 (structure height/width) using conventional photolithography techniques. Plating molds 40 μm in depth were obtained using a photosensitive polyimide (Probimide 349, OCG Micoelectronic Materials). The top magnetic cores and structures were then plated after removing the chromium layer on the bottom of plating molds. Upon completion of the top core electroplating, the photosensitive polyimide and chromium seed layer were removed.

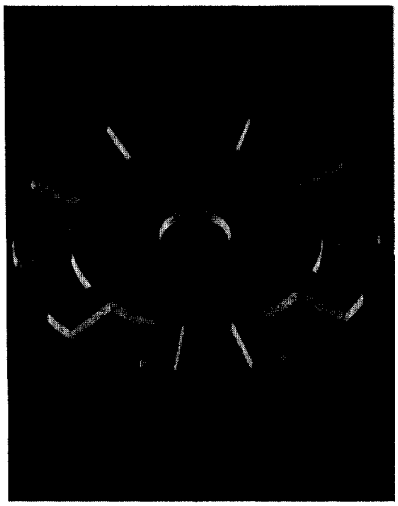

Fig. 6. Scanning electron micrograph of the fabricated rotor, where the outer diameter is 500 μm and the thickness is 40 μm.

The final thickness of the stator relative to the substrate was approximately 120 μm. Bonding pads were then opened in the polyimide layers by using the via etch process sequence described earlier. Optionally, to remove the chromium/copper/chromium plating seed layer located underneath the polyimide, the structure was dry etched to the bottom, and the chromium/copper/chromium was then selectively wet etched. It should be noted that removal of the magnetic core plating base was not required for successful device performance (this is a benefit of the meander inductor geometry).

In a separate process, 40-μm-thick nickel–iron rotors 500 μm in diameter were plated separately using the same photosensitive process described earlier and a chromium (500 Å)/copper (1 μm)/chromium (700 Å) sacrificial seed layer. These rotors were released from the substrate and assembled with stators. A scanning electron micrograph of the fabricated rotor is shown in Fig. 6. Fig. 7 shows a photomicrograph and a scanning electron micrograph of the assembled planar variable reluctance magnetic micromotor, which has an outer stator diameter of 1400 μm. A uniform gap separation of approximately 5–10 μm between the rotor and the stator is shown in Fig. 8. To ensure the rotation of rotor without touching on the stator poles, the gap separation between the rotor and the pin should be smaller than the gap separation between the rotor and the stator. The gap separation of approximately 5–10 μm between the rotor and the pin as well as the stator is shown in Fig. 9. Upon completion of the fabrication, samples were diced and bonded for test. The micromotor mounted on a package to test is shown in Fig. 10.

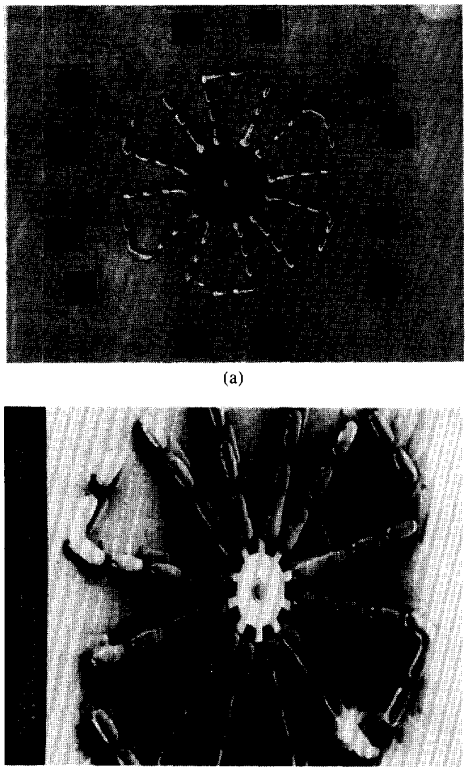

(a) (b)

Fig. 7. Photomicrograph and scanning electron micrograph of the fully fabricated micromotor: (a) photomicrograph; (b) scanning electron micrograph.

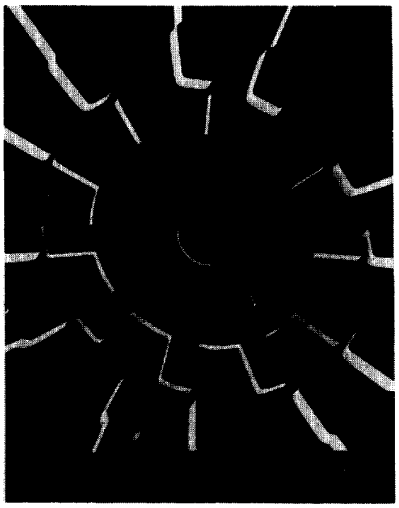

Fig. 8. Scanning electron micrograph of the assembled rotor and stator. An uniform gap separation of 5–10 μm between the rotor and the stator is shown.

V. Torque Evaluation

For a torque analysis in the magnetic motor, Fig. 11 shows a simple magnetic motor which can rotate about the axis with an instantaneous angle θ. When a current is

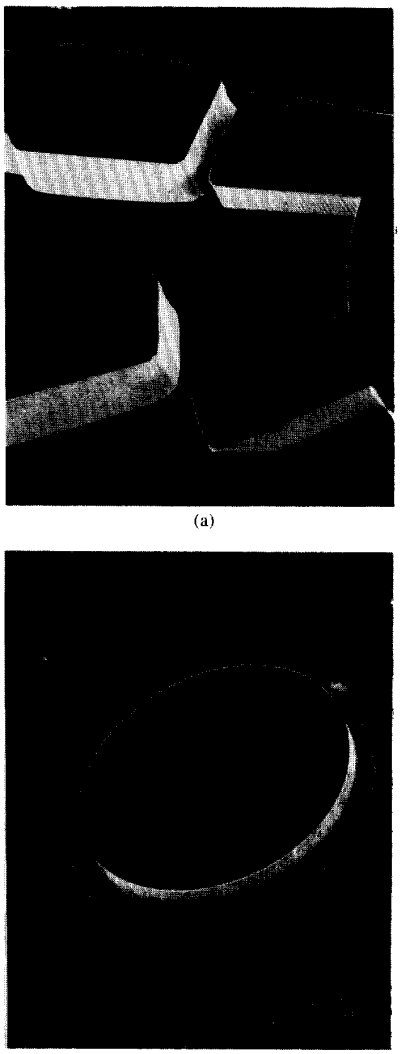

(a) (b)

Fig. 9. Gaps shown from the scanning electron micrograph of the assembled stator and rotor: (a) stator poles (left) and rotor poles (right), where approximately 5–10 μm gap separation is observed; (b) round pin in the diameter of 100 μm, where approximately 5–10 μm space between the pin and the rotor is observed.

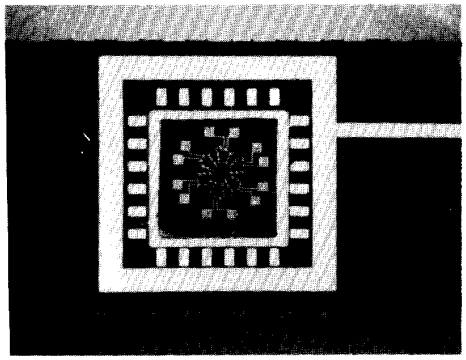

Fig. 10. Photomicrograph of the magnetic micromotor mounted on package.

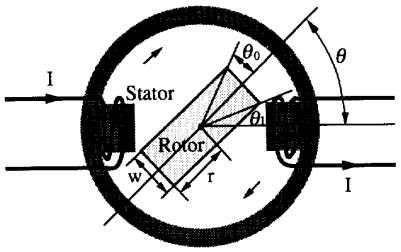

Fig. 11. Schematic diagram of a simple magnetic motor which can rotate about a central axis with an instantaneous position angle θ. Air gap: g; rotor radius: r; core length: l_c; coil turns: N.

applied to the phase winding, the rotor tends to align with the stator poles. A torque is produced to move the rotor to a minimum-reluctance position.

When the rotor rotates with an instantaneous angle θ, the superposed area (A_g) between the rotor pole and the stator pole is varied as

$$A_g = rt(2\theta_0 - \theta) \tag{4}$$

where r and t are the radius and the thickness of the rotor, respectively.

The reluctance of the magnetic circuit varies as a function of θ. In the magnetic circuit shown in Fig. 11, the reluctance of the magnetic core cannot be neglected due to a long magnetic path and a low magnetic permeability in the core. In contrast to the conventional motor, the core reluctance has a comparable value to the reluctance of the air gap. Consequently, the total reluctance ($R_\phi(\theta)$) in the magnetic circuit is the summation of the reluctances from the air gap (R_{gap}) and the magnetic core (R_{core}), which are expressed as

$$R_{\text{gap}} = \frac{2g}{\mu_0 A_g} = \frac{2g}{\mu_0 rt(2\theta_0 - \theta)} \tag{5}$$

$$R_{\text{core}} = \frac{(l_t - 2g)}{\mu A_c} = \frac{(l_t - 2g)}{\mu tW} \tag{6}$$

and

$$R_\phi(\theta) = R_{\text{gap}} + R_{\text{core}} = \frac{2g}{\mu_0 rt(2\theta_0 - \theta)} + \frac{(l_t - 2g)}{\mu tW} \tag{7}$$

where g is the air gap separation, W is the width of the magnetic core, and l_t is the total length of the magnetic path including air gap.

The inductance L will be varied between minimum and maximum values as the rotor rotates. The maximum inductance occurs when the rotor and stator poles are aligned and the minimum inductance occurs when a rotor interpolar axis is aligned with the stator poles. Thus the inductance $L(\theta)$ varies with instantaneous rotor position θ, which gives

$$L(\theta) = \frac{N^2}{R_\phi(\theta)} \tag{8}$$

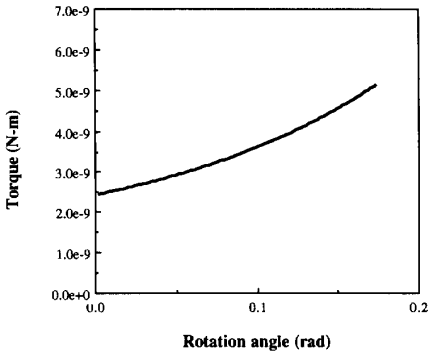

Fig. 12. Variation of the produced torque as a function of the rotor angle when a current of 500 mA is applied.

$$L(\theta) = \frac{N^2\mu_r\mu_0 rtW(2\theta_0 - \theta)}{2g\mu_r W + (l_t - 2g)r(2\theta_0 - \theta)} \quad \text{at} \quad \theta_1 < \theta < 2\theta_0 \tag{9}$$

$$L(\theta) = \frac{N^2\mu_r\mu_0 rtW\theta_0}{g\mu_r W + (l_t - 2g)r\theta_0} \quad \text{at} \quad 0 < \theta < \theta_1. \tag{10}$$

If it is assumed that the magnetic saturation is negligible and the linear relationship between flux linkage and driving current is valid at the instantaneous rotor position θ, the produced torque at the rotor is

$$T(\theta) = \frac{1}{2} i^2 \frac{\partial L(\theta)}{\partial \theta} \tag{11}$$

where i is the applied current to the stator coil. By substituting (10) into (11), the produced torque at $\theta_1 < \theta < 2\theta_0$ is

$$T(\theta) = \frac{1}{2} i^2 \frac{2g\mu_r^2\mu_0 N^2 rtW^2}{(2g\mu_r W + 2gr\theta + l_t(2\theta_0 - \theta)r - 4gr\theta_0)^2}. \tag{12}$$

The variation of the produced torque as a function of the rotor angle is shown in Fig. 12, using (12) and the same geometrical dimension as the micromotor designed in this research. The estimated torque is varied in the range of approximately 3.0–5.0 nN-m as shown in Fig. 12.

A rough estimate of the maximum attainable torque is also derived using an idealized maximum available energy conversion by Harris [18], [19] as

$$T = (\text{vol}) \frac{N_r B_s^2(\lambda - 1)q\beta g}{2\pi\mu_0 r_1} \tag{13}$$

where (vol) is the rotor volume, B_s is the magnetic flux density in the stator poles at the maximum flux linkage in the aligned position, λ is the aligned/unaligned unsaturated inductance ratio, β is the pole arc (assumed stator and rotor have the same arc), and g is the air gap. In the following section, based on the fabricated micromotor ge-

ometry and the measured electrical parameters, the achievable torque will be evaluated from (13) and compared with the torque evaluated from (12).

VI. Micromotor Performance

In the fabricated micromotor as shown in Fig. 7, the measured resistance of a single coil was approximately 1.5 Ω. A test of the maximum current that these coils could withstand was performed. Continuous currents of between 2.5 and 3 A could be sustained. Coil failure was not observed until continuous current reached over 4 A.

The inductance of a stator coil at 2 kHz is measured at the aligned position as well as the misaligned position of rotor poles with the stator poles. The maximum inductance measured at the aligned position is 0.232 μH and the minimum inductance measured at the misaligned is 0.225 μH. Thus, the inductance ratio (aligned/unaligned) λ is approximately 1.0131 (based on the measured values) assuming an air gap of 5 μm. Using a relative permeability μ_r of 500, and a saturation flux density of 0.5 T as mentioned in the previous section, the predicted torque from (13) is estimated as approximately 3.3 nN-m for a stator current of 500 mA. This value is of the same order of magnitude as the value plotted in Fig. 12, which was obtained from (12).

The first test of micromotor operation was to observe stepping action as phases were sequentially excited. Fig. 13 shows the result of this experiment. In Fig. 13(a), the rotor is shown in a position which is misaligned in comparison to the phase which is to be activated. Upon application of 500 mA to the active phase, rotational actuation was observed as shown in Fig. 13(b). The rotor has aligned exactly to the active phase as predicted. This experiment shows that the magnetic actuation is working well.

The next test was to sustain a continuous rotation of the rotor. The simple excitation apparatus used to drive the micromotor is described below. In order to protect the micromotor under test by limiting the maximum power dissipation, a standard curve tracer was used as a DC power source. A mechanical rotary switch driven by a variable speed AC motor was used to generate a three phase DC square wave. The frequency of the three phase square waves could be adjusted by varying the speed of the AC motor, thus controlling the rotation speed of the micromotor under test.

The three phase square waves generated from the rotary switch were then applied to the corresponding stator windings. Pole pairs in the same phase were connected so as to minimize the path length of the magnetic flux in the rotor. Applied currents of 200–500 mA with a driving voltage less than 1 V were sufficient to initiate motion from rest. Either by changing the phase firing order and keeping the micromotor connections constant or by exchanging two of the phase connections of the micromotor and keeping the phase firing order constant, the direction of rotation of the magnetic micromotor could be changed reversibly.

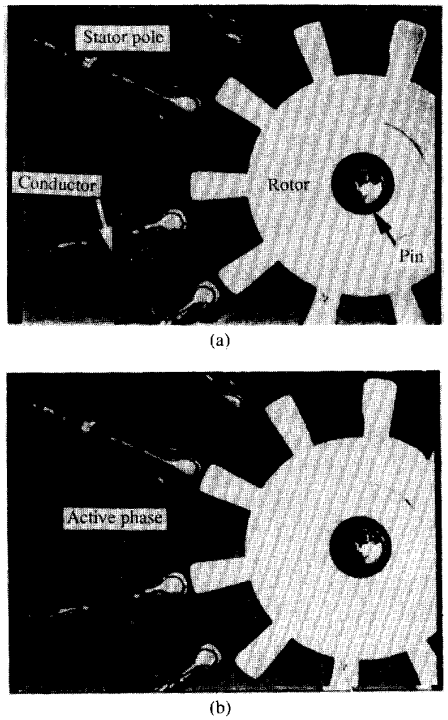

Fig. 13. Photomicrograph of the actuated rotor. When 500 mA of current was applied to each stator phase, 12° of rotation (1 stroke in this motor) was observed. (a) Before current is applied; (b) after current is applied, rotor poles are aligned to the stator poles of the active phase.

Although the maximum frequency of the driving pulse (and therefore the maximum micromotor speed) was limited by the mechanical rotary switch, the micromotor could be reproducibly started, stopped, reversed, and continuously rotated at speeds up to 500 rpm. It is fully expected that using electronic motor drive controllers, speeds in the thousands of rpm will be attainable. Such drive electronics are currently under development.

VII. Conclusions

A planar variable reluctance magnetic micromotor has been demonstrated on a silicon wafer with a micromachined nickel–iron rotor and a fully integrated stator, in which a meander type integrated inductive component has been used as the basic component for stator flux generation. A modified geometry from the conventional variable reluctance motor was utilized in order to minimize core reluctance. When 500 mA of current with a driving voltage less than 1 V was applied to each stator, 12° of rotation (1 stroke in this motor) was observed. The micromotor could be reproducibly started, stopped, reversed, and continuously rotated at speeds up to 500 rpm. The rotation speed was limited to 500 rpm by the driving controller used. Drive electronics capable of higher speeds are currently under development. The predicted torque for the fabricated micromotor at 500-mA drive current was approximately 3.3 nN-m.

ACKNOWLEDGMENT

The authors would like to thank Dr. A. B. Fraizer for his technical support on the photosensitive polyimide processing. Microfabrication was carried out at the Microelectronics Research Center (MiRC) of the Georgia Institute of Technology. The authors wish to thank the MiRC staff for their assistance. The authors would also like to gratefully acknowledge DuPont and OCG Microelectronics Materials for their donations of polyimide and Lake Shore Cryotronics, Inc., for their assistance in measurements of the magnetic properties of the permalloy thin films.

REFERENCES

[1] L. S. Fan, Y. C. Tai, and R. S. Muller, "IC-processed electrostatic micromotors," *Sensors and Actuators*, vol. 20, pp. 41–47, 1989.

[2] M. Meheregany, P. Nagarkar, S. D. Senturia, and J. H. Lang, "Operation of microfabricated harmonic and ordinary side-drive motors," in *Proc. IEEE Microelectromech. Syst. Workshop*, 1990, pp. 1–8.

[3] K. R. Udayakumar, S. F. Bart, A. M. Flynn, J. Chen, L. S. Tavrow, L. E. Cross, R. A. Brooks, and D. J. Ehrlich, "Ferroelectric thin film ultrasonic micromotor," in *Proc. IEEE Microelectromech. Syst. Workshop*, 1991, pp. 109–113.

[4] S. F. Bart and J. H. Lang, "An analysis of electroquasistatic induction micromotors," *Sensors and Actuators*, vol. 20, pp. 97–106, 1989.

[5] B. Wagner, M. Kreutzer, and W. Benecke, "Linear and rotational magnetic micromotors fabricated using silicon technology," in *Proc. IEEE Microelectromech. Syst. Workshop*, 1992, pp. 183–189.

[6] H. Guckel, K. J. Skrobis, T. R. Christenson, J. Klein, S. Han, B. Choi, E. G. Novell, and T. W. Chapman, "On the application of deep X-ray lithography with sacrificial layers to sensor and actuator construction (The magnetic micromotor with power takeoffs)," in *Proc. Transducers '91, 6th Int. Conf. Solid-State Sensors and Actuators*, Late News, 1991.

[7] H. Guckel, T. R. Christenson, K. J. Skrobis, T. S. Jung, J. Klein, K. V. Hartojo, and I. Widjaja, "A first functional current excited planar rotational magnetic micromotor," in *Proc. IEEE Microelectromech. Syst. Workshop*, 1993, pp. 7–11.

[8] C. H. Ahn and M. G. Allen, "A new toroidal-meander type integrated inductor with a multilevel meander magnetic core," *IEEE Trans. Magnetics*, vol. 30, no. 1, 1994.

[9] C. H. Ahn and M. G. Allen, "A fully integrated surface micromachined magnetic microactuator with a multilevel meander magnetic core," *IEEE J. Microelectromech. Syst.*, vol. 2, no. 1, pp. 15–22, 1993.

[10] C. H. Ahn, Y. J. Kim, and M. G. Allen, "A planar variable reluctance micromotor with fully integrated stator and wrappped coils," in *Proc. IEEE Microelectromech. Syst. Workshop*, 1993, pp. 1–6.

[11] C. H. Ahn, "Micromachined components as integrated inductors and magnetic microactuators," Ph.D. dissertation, Georgia Inst. Technology, Atlanta, GA, 1993.

[12] I. W. Wolf, "Electrodeposition of magnetic materials," *J. Appl. Phys.*, vol. 33, no. 3, pp. 1152–1159, 1962.

[13] R. D. Maclnnis and K. V. Gow, "Tensile strength and hardness of electrodeposited nickel-iron foil," *Plating*, pp. 135–136, 1971.

[14] M. E. Henstock and E. S. Spencer-Timms, "The composition of thin electrodeposited alloy films with special reference to nickel-iron," in *Proc. 6th Int. Metal Finishing Conf.*, 1963, pp. 179–185.

[15] Z. Nami, C. H. Ahn, and M. G. Allen, "Magnetic analysis of an overlapped cantilever beam magnetic microactuator using finite elements," *ASME*, DSC-vol. 46, Micromech. Syst., pp. 1–6, 1993.

[16] J. R. Hendershot, Jr., "Switched reluctance brushless DC motor with low loss magnetic circuits," in *Proc. Sixteenth Int. Intellig. Motion Conf.*, Long Beach, CA, 1989.

[17] A. B. Frazier and M. G. Allen, "High aspect ratio electroplated microstructures using a photosensitive polyimide process," in *Proc. IEEE Microelectromech. Syst. Workshop*, 1992, pp. 87–92.

[18] M. R. Harris, "Static torque production in saturated doubly-salient machines," *Proc. Inst. Elec. Eng.*, vol. 122, pp. 1121–1127, 1975.

[19] T. J. E. Miller, *Brushless Permanent-Magnet and Reluctance Motor Drives*. Oxford, New York: Clarendon, 1989.

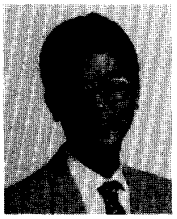

Chong H. Ahn received the B.S. degree in electrical engineering from Inha University, South Korea, in 1980, the M.S. degree in electrical engineering from Seoul National University, South Korea, in 1983, and the Ph.D. degree in electrical and computer engineering from the Georgia Institute of Technology in 1993.

He is currently a postdoctoral fellow at the Microelectronics Research Center, School of Electrical and Computer Engineering, Georgia Institute of Technology, Atlanta, GA. His research interests include the development, design, fabrication, and characterization of fully integrated microsensors and microactuators; micromachined planar inductive components; planar magnetic micromotors; and integrated dc/dc converters, using microfabrication technologies.

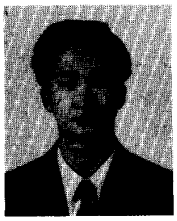

Yong J. Kim received the B.S. degree in electrical engineering from Yonsei University, Seoul, Korea, in 1987, and the M.S. degree in electrical engineering from the University of Missouri-Columbia, in 1989. He is now working towards the Ph.D. degree at the School of Electrical and Computer Engineering, Georgia Institute of Technology. His research includes microactuators using magnetic components, applications of electroless plating technique in micromachining, and the investigation of the mechanical properties of polyimides.

Mark G. Allen received the B.A. degree in chemistry, the B.S.E. degree in chemical engineering, and the B.S.E. degree in electrical engineering from the University of Pennsylvania in 1984, and the S.M. degree in 1986 and the Ph.D. degree in 1989, both from the Massachusetts Institute of Technology.

Since 1989 he has been an Assistant Professor in the School of Electrical and Computer Engineering at the Georgia Institute of Technology. His research includes micromachining fabrication technology, microoptomechanical systems, and material issues in micromachined structures and electronic packages.

Dr. Allen is a member of the editorial board of the *Journal of Micromechanics and Microengineering*.